The Toughening Effect and Mechanism of Styrene–Butadiene Rubber Nanoparticles for Novolac Resin

Wei-Wei Liu, Jing-Jing Ma, Mao-Sheng Zhan, Kai Wang

School of Material Science and Engineering, Beihang University, Beijing 100191, People's Republic of China
Correspondence to: M.-S. Zhan (E-mail: zhanms@buaa.edu.cn)

ABSTRACT: In this article, phenolic nanocomposites were prepared using styrene–butadiene rubber (SBR) nanoparticles with an average particle size of about 60 nm as the toughening agent. The mechanical and thermal properties of phenolic nanocomposites and the toughening mechanism were studied thoroughly. The results showed that when adding 2.5 wt % SBR nanoparticles, the notched impact strength of phenolic nanocomposites reached the maximum value and was increased by 52%, without sacrificing the flexural performance. Meanwhile, SBR nanoparticles had no significant effect on the thermal decomposition temperature of phenolic nanocomposites. The glass-transition temperature (T_g) of phenolic nanocomposites shifted to a lower temperature accompanying with the increasing T_g of loaded SBR, which showed there was a certain compatibility between SBR nanoparticles and phenol-formaldehyde resin (PF). Furthermore, the analysis of Fourier transform infrared spectroscopy and X-ray photoelectron spectroscopy indicated that there existed a weak chemical interaction between SBR nanoparticles and the PF matrix. The certain compatibility and weak chemical interaction promoted the formation of a transition layer and improved the interfacial bonding, which might be important reasons for the great enhancement of the toughness for phenolic nanocomposites. © 2014 Wiley Periodicals, Inc. J. Appl. Polym. Sci. **2015**, *132*, 41533.

INTRODUCTION

Phenol-formaldehyde resin (PF) is a kind of typical thermosetting resin with highly crosslinked network structure, so their application has been significantly limited by inherent brittleness. Currently, internal and external toughening are two main methods to improve the toughness of PF. In the internal toughening method, flexible molecular chains are introduced into PF to change the molecular structure. Materials, such as suberic acid,[1] epoxidized soybean oil,[2] and cardanol,[3] have been used as internal toughening agents. External toughening method means adding toughening agents to the synthesized PF. The toughening agents are physically mixed with PF, accompanied by a small number of chemical reactions sometimes. Materials, such as poly(2-ethyl hexyl acrylate),[4] nitrile rubber,[5] polyamides,[6] and p-hydroxyphenylmaleimide (HPMI)/acrylic ester copolymer,[7] have been used as external toughening agents. Compared with the internal toughening, external toughening has a wider range of applications because of its simplicity and low-cost. However, external toughening usually sacrifices the heat resistance, flexural strength, and modulus of materials while gaining good toughening effect.

There have been some studies choosing elastomeric nanoparticles as toughening agents, in which toughness, flexural

strength, and heat resistance of composites were improved simultaneously. Phenolic nanocomposites modified by nitrile butadiene elastomeric nanoparticles (NBENP) and carboxylic nitrile butadiene elastomeric nanoparticles (CNBENP) have been investigated by Qiao and coworkers.[8] In their study, the impact strength of phenolic nanocomposites with 5 wt % NBENP or CNBENP was increased by 49 and 67%, respectively. The flexural strength was also improved. The uniform dispersion of rubber particles in the PF matrix with a diameter of about 100 nm and the influence of rubber particles on some hydrogen bonds and phenolic hydroxyl groups, contributed to the enhancement of interfacial adhesion between PF and rubber particles and further led to the increase of the impact strength. In addition, in the research of phenolic resin toughened by nanocarboxylic acrylonitrile butadiene rubber latex (XNBRL),[9] Chen et al. found that the impact strength of PF with 10 wt % of XNBRL was increased by 127%. Moreover, the study indicated that the XNBRL was uniformly dispersed in the PF matrix with diameters ranging from 200 to 400 nm. A chemical reaction occurred between —COOH of XNBRL and —CH$_2$OH of PF. In addition, CNBENP was used as the toughening agent of epoxy resin.[10,11] In this case, when the content of CNBENP was 12 phr, the impact strength, heat distortion temperature, and T_g
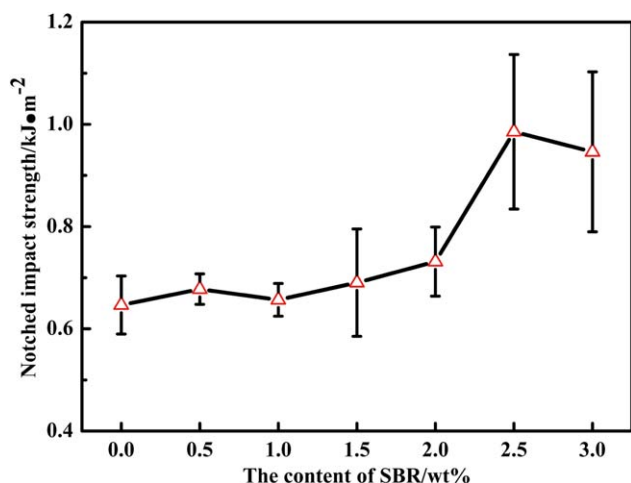
Figure 1. The notched impact strength of phenolic nanocomposites with various SBR contents. [Color figure can be viewed in the online issue, which is available at wileyonlinelibrary.com.]

Figure 3. The thermogravimetric curves of SBR, PF, and PF/SBRX ($X = 0.5$, 1.5, 2.5, 3.0). [Color figure can be viewed in the online issue, which is available at wileyonlinelibrary.com.]

of the modified epoxy resin were increased by 96, 1.1, and 3.5%, respectively. And it was confirmed that the nitrile group participated in the curing reaction of the epoxy resin using DSC and *in situ* FTIR. The interaction between the nitrile group and the epoxy resin resulted in the formation of a harder interface, which increased both toughness and heat resistance of the modified epoxy resin. The above analysis indicated that nitrile rubber (NBR) nanoparticles were a kind of effective external-toughening agent. The interfacial interaction between elastomeric nanoparticles and the matrix was a critical factor in the improvement of toughness. However, NBR must be modified to improve the compatibility between NBR and PF, thus increasing the cost and limiting the application of composites. Recently, Faghihi et al.[12] discovered that the T_g of styrene–butadiene rubber (SBR) shifted more to the higher temperature than NBR in the mixtures of PF and SBR or NBR, which might be associated with a better compatibility.
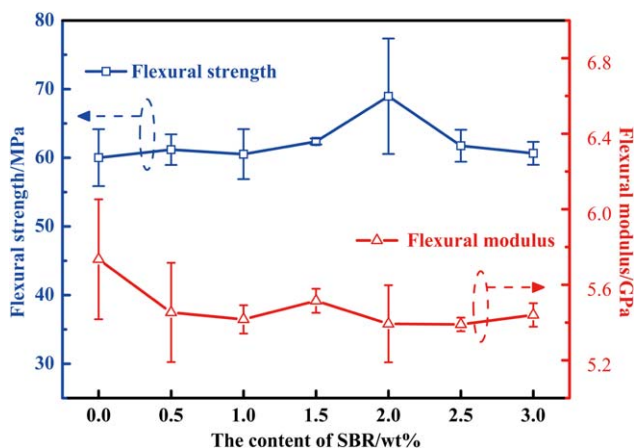
Therefore, in this work, we selected SBR nanoparticles as the toughening agent of PF and studied the toughening effect and mechanism of SBR nanoparticles for PF. To start with, the mechanical and thermal properties of phenolic nanocomposites were investigated. Second, the toughening mechanism was

Figure 2. The flexural properties of phenolic nanocomposites with various SBR contents. [Color figure can be viewed in the online issue, which is available at wileyonlinelibrary.com.]
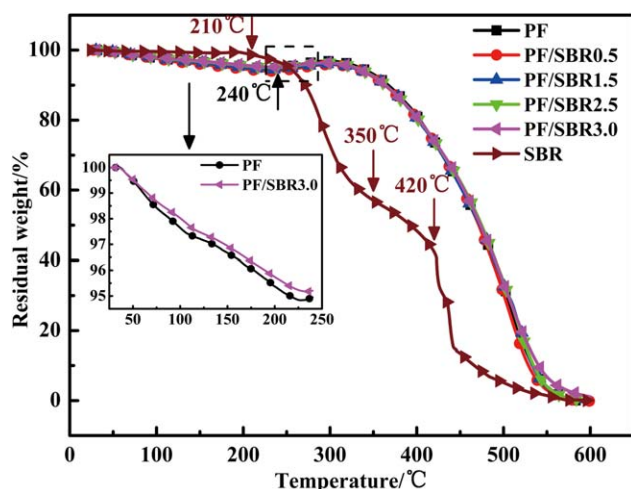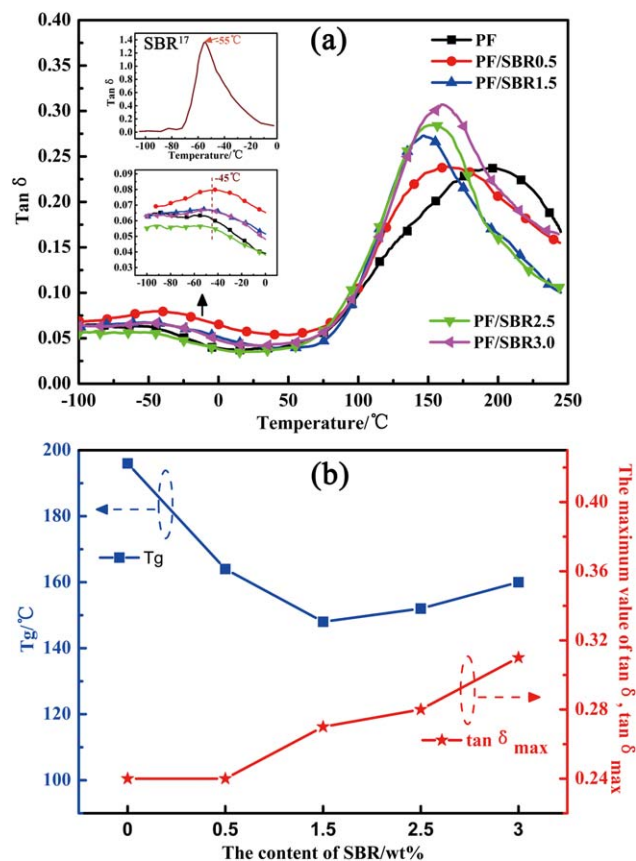
Figure 4. DMTA test results of PF and PF/SBRX ($X = 0.5$, 1.5, 2.5, 3.0). [Color figure can be viewed in the online issue, which is available at wileyonlinelibrary.com.]
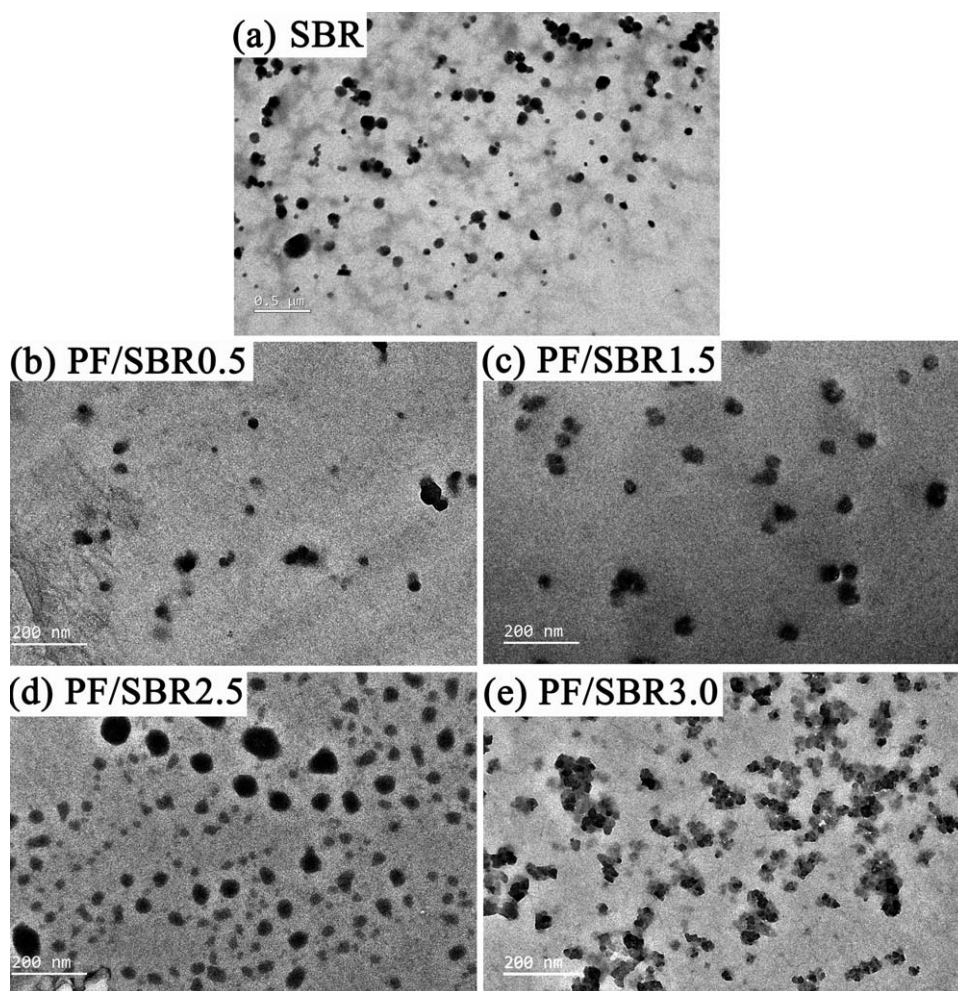
Figure 5. TEM images of SBR and PF/SBR nanocomposites.

studied by glass-transition temperature, aggregation structure, and chemical structure using dynamic mechanical analyzer (DMA), transmission electron microscope (TEM), Fourier transform infrared spectroscopy (FTIR), and X-ray photoelectron spectroscopy (XPS).

EXPERIMENTAL

Materials

PF, an oxalic acid catalyzed novolac resin, is cured by hexamethylenetetramine (HMTA). PF and HMTA are both provided by Ningbo Anli Electronic Materials Co., wherein PF is a kind of slight yellow transparent solid and HMTA is a kind of white powder. SBR nanoparticles with average particle size about 60 nm are prepared from a special irradiation technique[13] and provided by the Beijing Research Institute of Chemical Industry.

Preparation of the Molded Samples

The PF, SBR nanoparticles, and HMTA were weighed proportionally and mixed in a FW100 high-speed mixer (24000 r/min, Tianjin Taisite Instrument Co., LTD). The content of HMTA was 11.1% by weight of PF. The proportions of SBR nanoparticles were 0.5, 1.0, 1.5, 2.0, 2.5, and 3.0 wt % with respect to PF. The mixtures were molded for 20 min at 180°C under a pressure of 9 MPa.[14] Molded samples of pure PF and phenolic

nanocomposites with different proportions of SBR were denoted as PF and PF/SBRX ($X = 0.5$, 1.0, 1.5, 2.0, 2.5, 3.0).

Characterization Methods

Characterization of Mechanical and Thermal Properties. The notched charpy impact strength of molded samples was measured by a LEIPZ16 impact machine. The dimensions of specimens are 60 mm $\times$ 10 mm $\times$ 4 mm and there is a 1 mm $\times$ 1 mm notch on the side of 4 mm. The distance between the supporting points is 40 mm. The three-point bending performances of molded samples were tested on an INSTRON-5565 universal material testing machine at a deformation rate of 1 mm/min. The size of samples is 60 mm $\times$ 10 mm $\times$ 4 mm. The radii of indenter (R1) and supports (R2) are both 5.0 mm $\pm$ 0.1 mm and the span is 40 mm. The thermogravimetric analysis of samples was performed with a Q5000IR thermo gravimetric analyzer (TA, America) from room temperature (RT) to 600°C at a rate of 10°C/min in synthetic air atmosphere.

Characterization of Glass Transition Temperature (T_g). The determination of T_g was conducted with a Q800 DMA (TA, America) from -100 to 250°C with heating rate of 5°C/min. Measurements were performed using a three-point bending
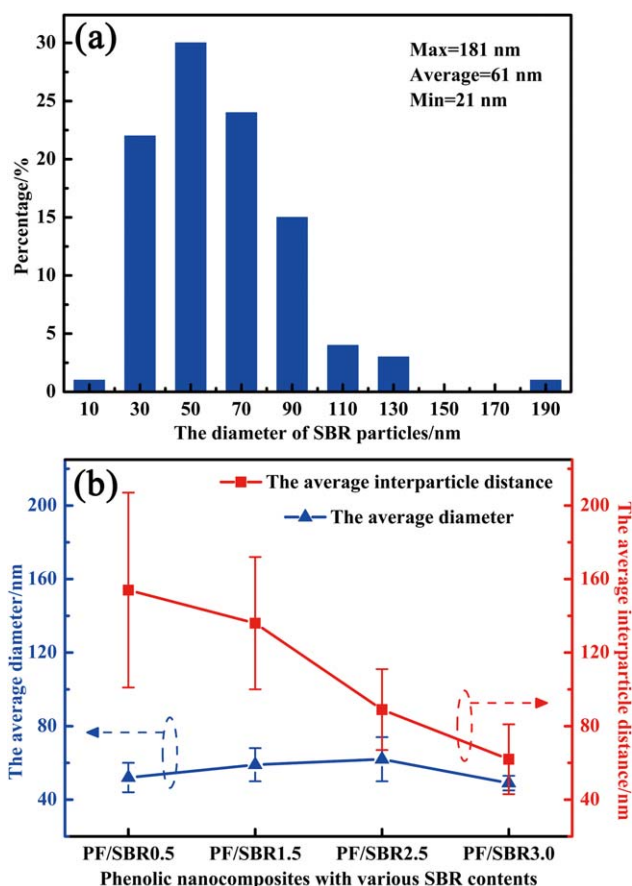
Figure 6. The diameter distribution of SBR nanoparticles (a) and the average diameter and average interparticle distance of SBR nanoparticles dispersed in the PF matrix (b). [Color figure can be viewed in the online issue, which is available at wileyonlinelibrary.com.]

mode at a frequency of 1 Hz. The specimens used for the test are of dimensions 40 mm $\times$ 4 mm $\times$ 2 mm. The peak of loss factor (tanδ) curve was taken as T_g.

Characterization of Aggregation Structure. TEM images were obtained from a JEM-3010 (JEOL, Japan) machine. SBR nanoparticles were dispersed into the ethanol solution and then the dispersion solution was dropped on a carbon film. The molded samples were ultramicrotomed at RT and stained in O_sO_4 vapor for 30 min. The morphologies of notched impact fracture surfaces were examined with a CS3400 scanning electron microscope (SEM). Samples were coated with a thin gold layer under vacuum.

Characterization of Chemical Structure. The *in situ* FTIR spectra were recorded using a Nicolet 6700 spectrometer (Thermo-Fisher, America) at a resolution of 4 cm^{-1} between 4000 and 400 cm^{-1}. The testing temperature ranged from RT to 300°C. XPS spectra were performed on an ESCALAB 250 spectrometer using a monochromated Al Kα X-ray source (150 W). A spot of 500 μm in diameter, 200 eV of pass energy for survey scan and 30 eV for high-resolution scan were used during analysis. A Gaussian-Lorentzian function was used for curve fitting O1s and C1s photopeaks. The C1s electron binding energy was referenced at 284.8 eV.

RESULTS AND DISCUSSION

Mechanical and Thermal Properties

Mechanical Properties. The notched impact strength of PF and PF/SBRX ($X = 0.5$, 1.0, 1.5, 2.0, 2.5, 3.0) is shown in Figure 1. The notched impact strength of phenolic nanocomposites with SBR is better than that of pure PF. When the loading of SBR is less than 1.5 wt %, the variation of the notched impact strength for phenolic nanocomposites is not obvious. When the loading of SBR is between 1.5 and 2.5 wt %, the notched impact strength of phenolic nanocomposites progressively increases and reaches the maximum value at the content of 2.5 wt % higher than that of PF/SBR3.0. The notched impact strength of PF/SBR2.5 is 0.99 kJ·m^{-2} and increased by 52% compared with pure PF. A study by Qiao and coworkers[8] claimed that the impact strength of phenolic nanocomposites with 5 wt % NBENP was increased by 49%. In contrast, our data indicate that better notched impact strength is achieved with a lower loading of elastomeric nanoparticles.

The flexural strength and modulus of phenolic nanocomposites with various SBR contents are given in Figure 2. The flexural strength of phenolic nanocomposites modified by SBR nanoparticles is higher than that of pure PF. For PF/SBR0.5, PF/SBR1.0, and PF/SBR1.5, the changes of flexural strength are slight. The flexural strength of PF/SBR2.0 reaches the maximum value, 69 MPa, and is increased by 15% compared with pure PF. The
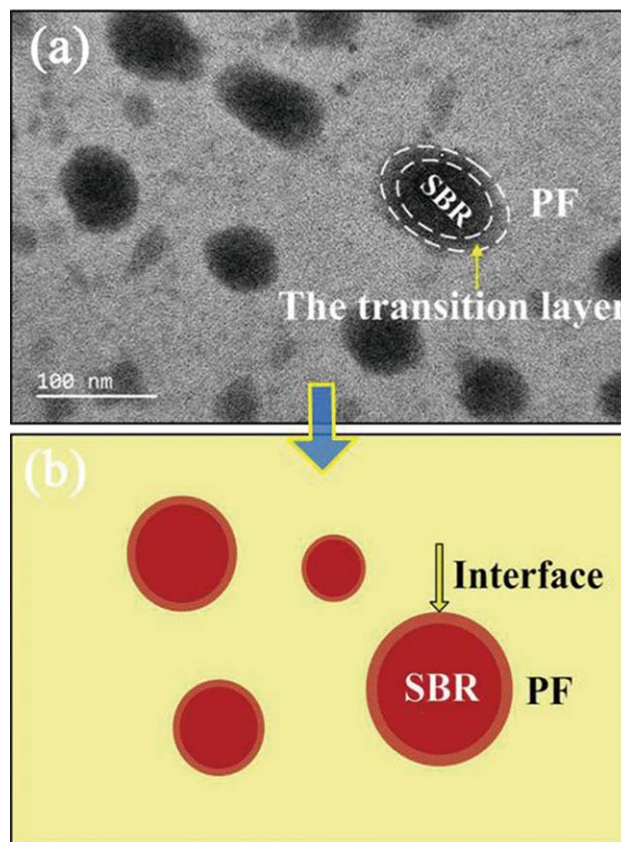

Figure 7. Magnified TEM image of PF/SBR2.5 disperse morphology (a) and the schematic illustration (b). [Color figure can be viewed in the online issue, which is available at wileyonlinelibrary.com.]
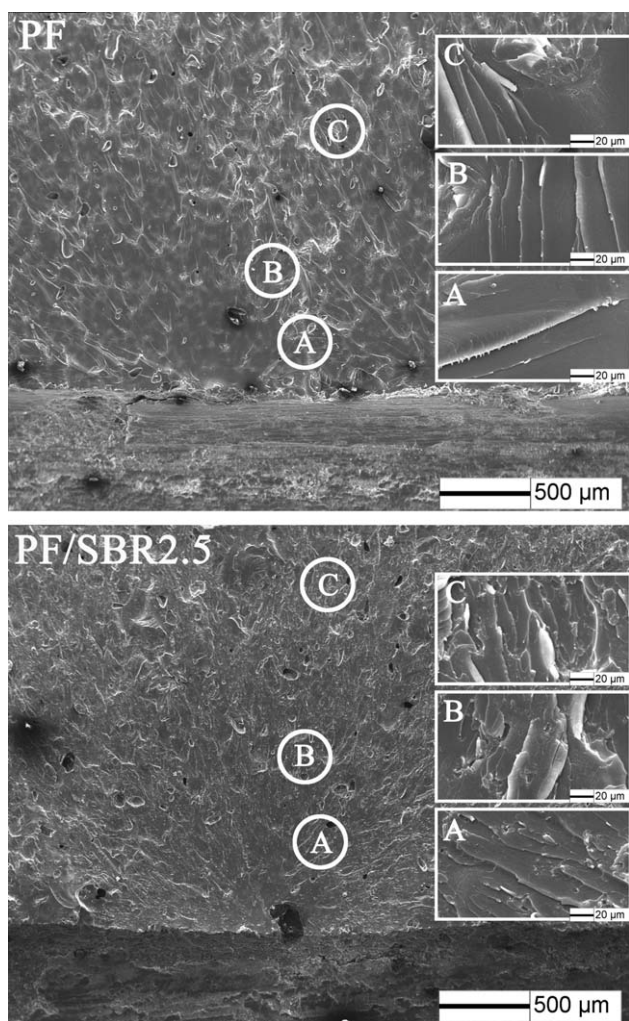
Figure 8. SEM images of notched impact fracture surfaces.

flexural modulus of phenolic nanocomposites with SBR nanoparticles is lower than that of pure PF. However, the decline of flexural modulus with the SBR content increasing is not evident. For PF/SBR3.0, the flexural modulus is decreased by only 5%. Therefore, phenolic nanocomposites with SBR nanoparticles have good impact strength and flexural performance. The good mechanical properties of phenolic nanocomposites may be associated with the interface between SBR nanoparticles and the PF matrix,[8,10] or the size and dispersion morphology of SBR nanoparticles,[15] which will be considered in the following study.

Thermal Property. Figure 3 shows the thermogravimetric curves of SBR, PF, and PF/SBRX ($X = 0.5$, 1.5, 2.5, 3.0). The thermogravimetric curve of SBR is divided into four stages. Below 210°C, SBR exhibits good heat resistance, indicating that the chemical structure of SBR is substantially not damaged. From 210 to 350°C, the fracture of SBR occurs,[16] which leads to a rapid weight loss of SBR. From 350 to 420°C, butadiene components are gradually depleted, thus the rate of weight loss is slow. Above 420°C, benzenes start to fracture and the weight loss of SBR accelerates again. The decomposition process analysis of SBR illustrates that SBR nanoparticles may damage the thermal property of phenolic nanocomposites at higher temper-

ature. However, the effect of SBR nanoparticles on the thermal decomposition temperature of phenolic nanocomposites is not obvious. The thermogravimetric curves of PF and PF/SBRX ($X = 0.5$, 1.5, 2.5, 3.0) almost overlap with each other and their trends are as follows. Below 240°C, the loss of weight is small, about 5%. From 240 to 300°C, weight increases slightly as shown in the rectangle. Above 300°C, weight loses rapidly. But it can be seen from the enlarged thermogravimetric curves of PF and PF/SBR3.0 below 240°C that PF/SBR3.0 has a larger residual weight, which reveals that the thermal property of PF/SBR3.0 at lower temperature is improved slightly. The analysis indicates that the thermal decomposition temperature of phenolic nanocomposites is not affected significantly, on the premise of improving toughness. The interface between SBR nanoparticles and the PF matrix may be a major factor for the good thermal property of phenolic nanocomposites.[8,10]

The Toughening Mechanism Analysis

The Analysis Based on T_g. Loss factor versus temperature curves of SBR,[17] PF, and PF/SBRX ($X = 0.5$, 1.5, 2.5, 3.0) are presented in Figure 4(a). There are two peaks in the plots of PF and PF/SBRX ($X = 0.5$, 1.5, 2.5, 3.0) and the T_g of SBR in the literature[17] is −55°C. The peaks at near −45°C, corresponding to the T_g of SBR in phenolic nanocomposites or the secondary transition of PF segments, reveal that the T_g of SBR in phenolic nanocomposites is higher than the T_g of SBR[17] or that the addition of SBR leads to a more obvious secondary transition of PF segments. Furthermore, the T_g of phenolic nanocomposites corresponding to the peaks at higher temperature and the values of $\tan\delta_{max}$ are displayed in Figure 4(b). The T_g of phenolic nanocomposites decreases from 196 to 160°C, which reveals that there is a tendency of compatibility between SBR nanoparticles and the PF matrix. At the same time, the value of $\tan\delta_{max}$ increases from 0.24 to 0.31, indicating the movement of PF segments becomes easier and the mechanical loss[12] increases. Given the above analysis, it is clear that there is a certain compatibility between SBR nanoparticles and the PF matrix, which plays a key role in the enhancement of impact strength.

The Analysis Based on Aggregation Structure. The TEM images of SBR and PF/SBRX ($X = 0.5$, 1.5, 2.5, 3.0) are presented in Figure 5(a–e). It can be seen that phenolic nanocomposites possess a two-phase structure with the uniform dispersion of SBR nanoparticles. When the content of SBR nanoparticles reaches 3 wt %, slight aggregation of SBR nanoparticles appears.

Moreover, as shown in Figure 6, Figure 6(a) indicates that the diameters of SBR nanoparticles themselves range from 21 to 181 nm with an average diameter of about 61 nm. More than 80% of SBR nanoparticles are less than 100 nm. Figure 6(b) shows that the average diameters of SBR nanoparticles in phenolic nanocomposites with various SBR contents are around 60 nm and the average interparticle distance in phenolic nanocomposites decreases from 154 to 43 nm with the increase of SBR content. Our data display that SBR nanoparticles are dispersed in the PF matrix at a nanoscale. Thus, the notched impact strength will be improved with the increase of SBR content because the interaction area between SBR nanoparticles
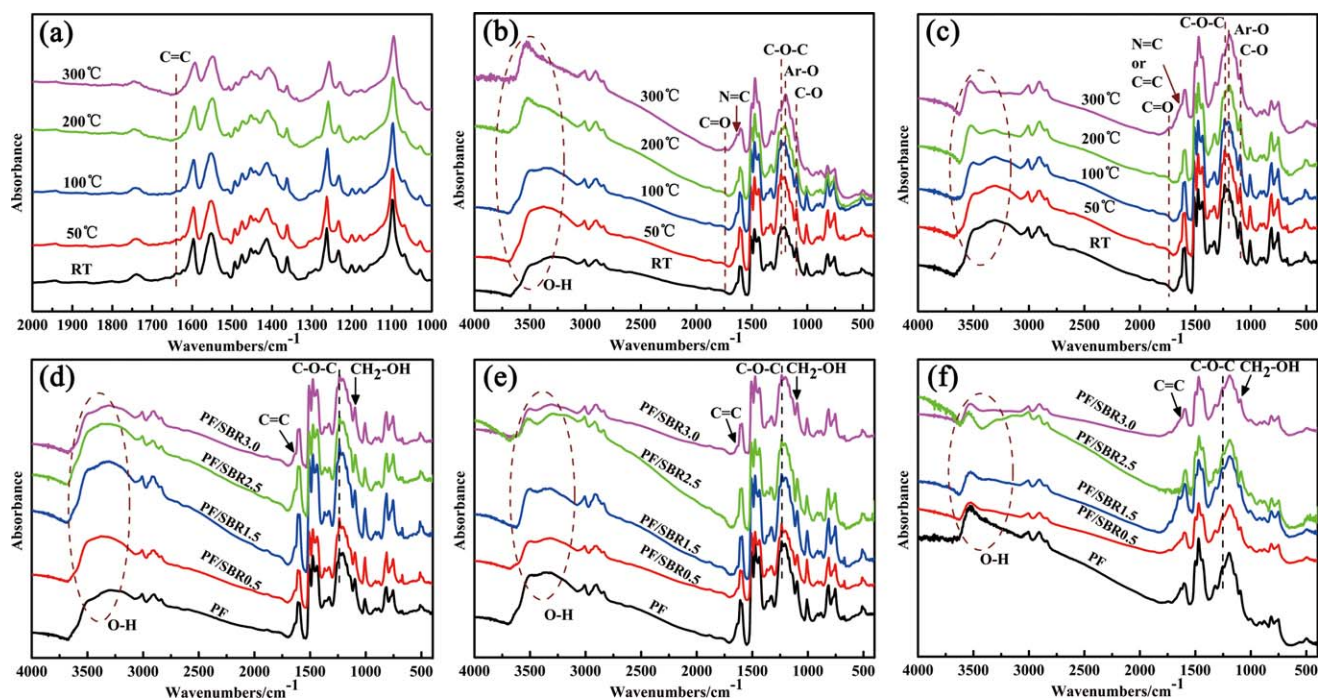
Figure 9. FTIR spectra: SBR, PF, and PF/SBR3.0 at different temperatures (a, b, c); PF and PF/SBRX ($X = 0.5, 1.5, 2.5, 3.0$) at room temperature, 100, and 300°C (d, e, f). [Color figure can be viewed in the online issue, which is available at wileyonlinelibrary.com.]

and the PF matrix increases and the average interparticle distance decreases. However, the notched impact strength of PF/SBR2.5 reaches the maximum value higher than that of PF/SBR3.0, which indicates that there is a critical interparticle distance between PF/SBR2.5 and PF/SBR3.0. When the average interparticle distance is greater than the critical value, the notched impact strength increases with the decrease of the average interparticle distance.[18] In contrast, the notched impact strength declines and slight aggregation of SBR nanoparticles appears in PF/SBR3.0 shown in Figure 5(e).

Meanwhile, in Figure 7(a), a transition layer with a thickness of about 15 nm between SBR nanoparticles and the PF matrix is observed in the TEM micrograph of PF/SBR2.5 at higher magnification. The schematic illustration is shown in Figure 7(b). The transition layer may be associated with a good interfacial bonding. Thus, phenolic nanocomposites with SBR nanoparticles have excellent impact strength. At the same time, the thermal decomposition temperature is not influenced significantly.

In addition, SEM micrographs of notched impact fracture surfaces for PF and PF/SBR2.5 are shown in Figure 8. The fracture surfaces of pure PF exhibit typical characteristics of brittle fracture and are relatively smooth with a clear radiation pattern. Although the roughness of phenolic nanocomposites with 2.5 wt % SBR nanoparticles increases and multiple crack layers appear, which indicates SBR nanoparticles play a role in initiating crack[19] and confirms the enhancement of the toughness for phenolic nanocomposites.

The Analysis Based on Chemical Action. FTIR and XPS are used to further analyze the compatibility and interfacial interaction between SBR nanoparticles and the PF matrix. The FTIR

spectra of SBR, PF, and PF/SBR3.0 at different temperatures are shown in Figure 9(a–c), whereas the FTIR spectra of RT, 100, and 300°C for PF and PF/SBRX ($X = 0.5, 1.5, 2.5, 3.0$) are displayed in Figure 9(d–f). The FTIR analysis is based on the main IR characteristic bands of SBR and cured PF presented in Table I. As shown in Figure 9(a), the band at 1640 cm^{-1} assigned to C=C gradually disappears as temperature increases, revealing that the C=C bonds remained in SBR are consumed. As for the

Table I. The Main IR Characteristic Bands of SBR and Cured PF

| Wavenumber/cm^{-1}	Corresponding characteristic bands
3312, 3503	Stretching vibration of phenolic hydroxyl groups: 3312 for associated hydroxyl groups, 3503 for free hydroxyl group[20]
3011	Ar—H stretching vibration
2906, 2838	—CH$_2$— antisymmetric and symmetric stretching vibration
1640	N=C or C=C stretching vibration
1612, 1595, 1507	C—C stretching vibration of aromatic ring
1471, 1437	In-plane scissor vibration of —CH$_2$— linking aromatic ring
1230	C—O—C stretching vibration
1206	C—O stretching vibration of Ar—OH
1100	C—O stretching vibration of —CH$_2$—OH[21]
1008	Ar—H in-plane bending vibration
880~672	Ar—H out-of-plane bending vibration
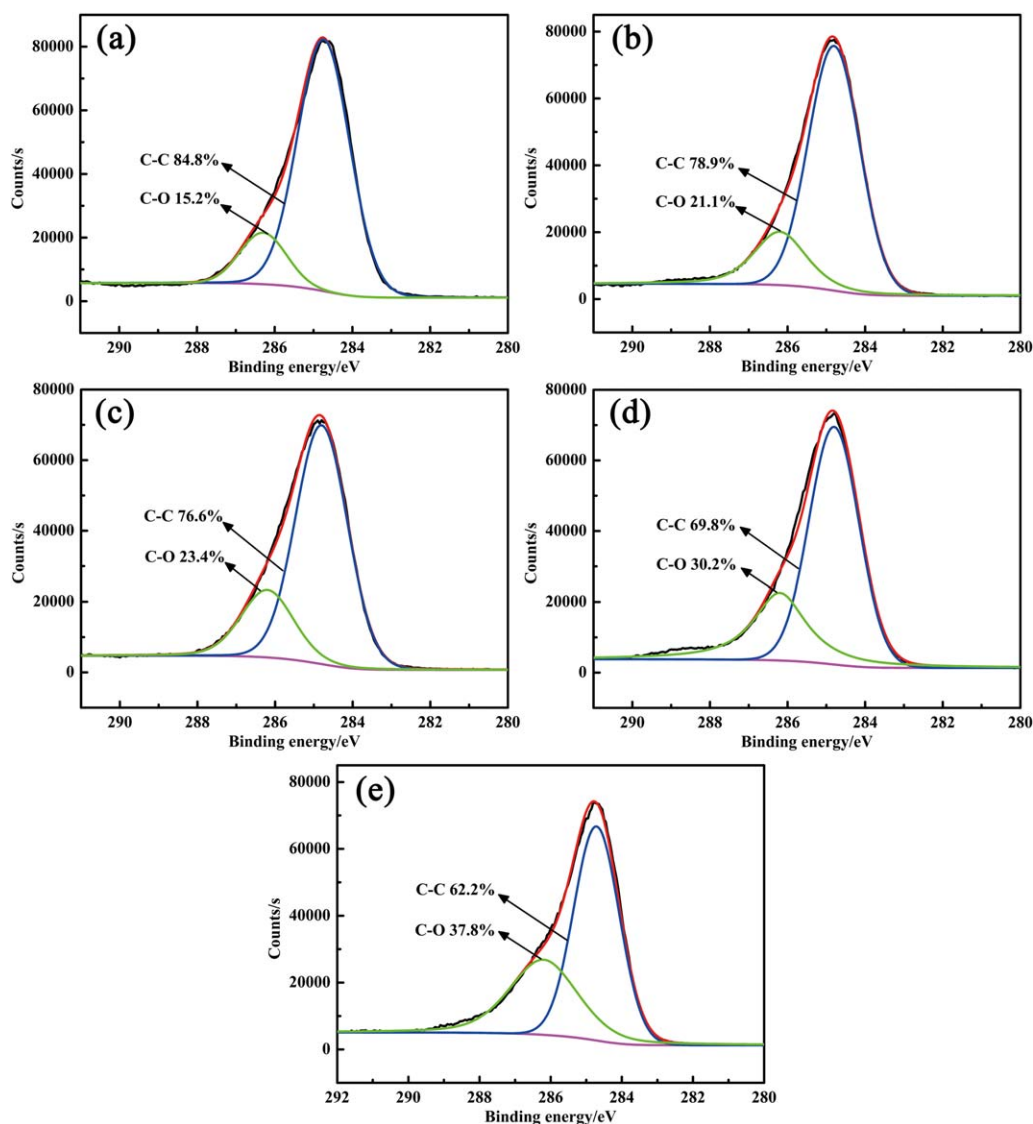
Figure 10. High-resolution C1s XPS spectra: (a) PF, (b) PF/SBR0.5, (c) PF/SBR1.5, (d) PF/SBR2.5, (e) PF/SBR3.0. [Color figure can be viewed in the online issue, which is available at wileyonlinelibrary.com.]

FTIR spectra of PF and PF/SBRX ($X = 0.5$, 1.5, 2.5, 3.0) at different temperatures, they exhibit similar changes. Therefore, only the FTIR spectra of PF and PF/SBR3.0 are displayed in Figure 9(b,c). It can be seen that the changes in structure are mainly in O—H, C—O—C, C—O of Ar-OH, C=O and C—O of —CH$_2$—OH, that is, four phenomena occur with the increase of temperature. (1) The broad peak of associated hydroxyl groups at 3312 cm^{-1} gradually disappears, whereas the peak of free hydroxyl groups at 3503 cm^{-1} increases and becomes a sharp peak. This means that the associated hydroxyl groups are broken, which produces sharp stretching vibration peak of free hydroxyl groups, or that the residual moisture in samples evaporates, which indicates that the vibrational and rotational peak of gaseous water (3503 cm^{-1}) appears. (2) The peak of C—O—C (1230 cm^{-1}) gradually disappears, indicating the breakage of ether bond in PF occurs. (3) The 1206 cm^{-1} band attributed to C—O of Ar—OH weakens and shifts to a lower

wavenumber (1189 cm^{-1}). And there is no significant change in the band of —CH$_2$—. However, a new peak appears at 1735 cm^{-1}, belonging to the stretching vibration of C=O. Overall, some phenolic hydroxyl groups are oxidized, which explains the slight weight increase from 240 to 300°C in the thermogravimetric curves of PF and PF/SBRX ($X = 0.5$, 1.5, 2.5, 3.0) (Figure 3). (4) The peak of C—O of —CH$_2$—OH becomes weaker, implying that the C—O bond may react with the C=C bond in SBR. Nevertheless, the reaction between C=C bond and —CH$_2$—OH group cannot be confirmed, because the band of N=C coincides with the band of C=C.

In addition, Figure 9(d–f) manifests that the structure of PF varies with the increase of SBR loading. Three main changes are included below: (1) The associated phenolic hydroxyl groups are split and the band of free hydroxyl groups at 3503 cm^{-1} increases progressively. Moreover, the above changes become more obvious with the increase of temperature, which is in
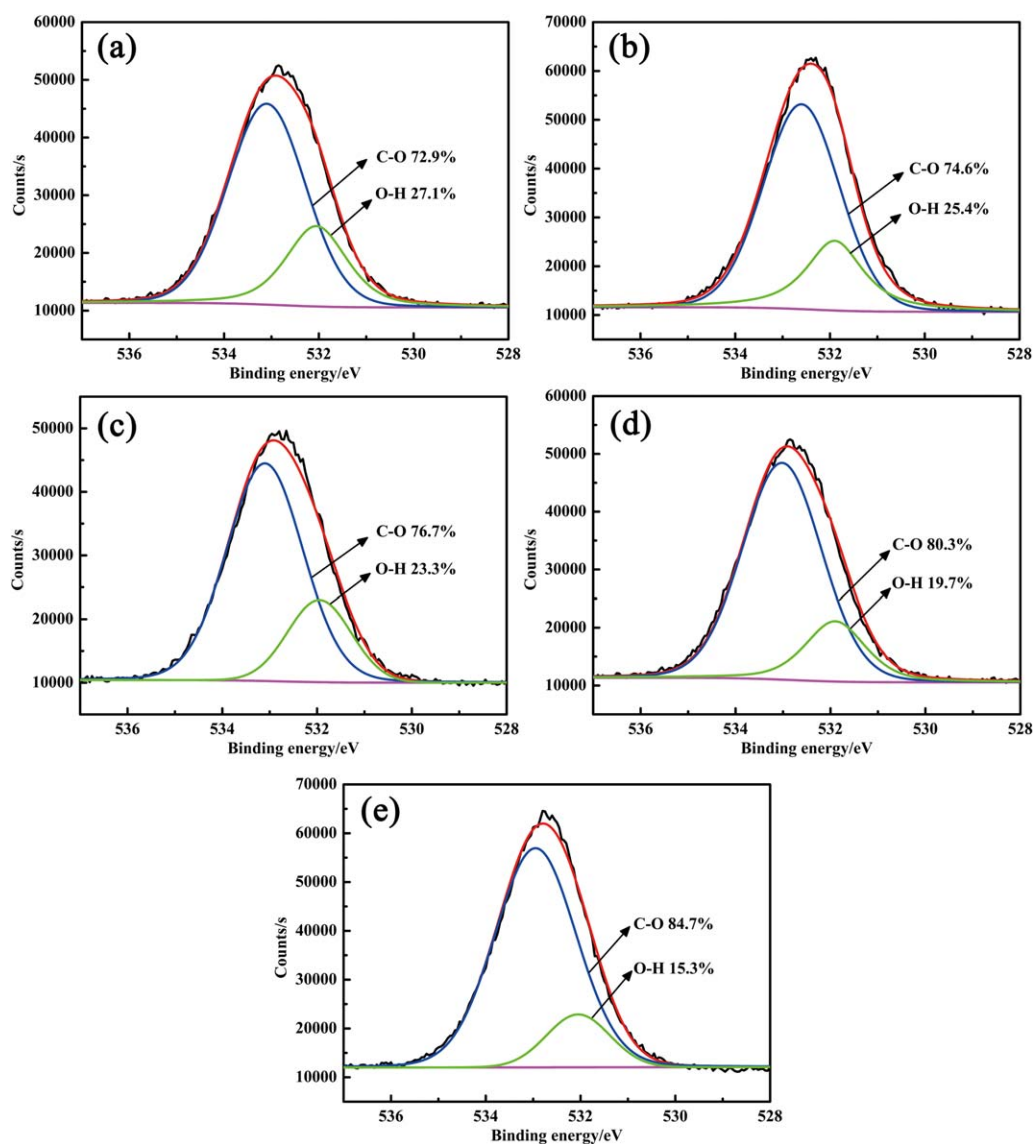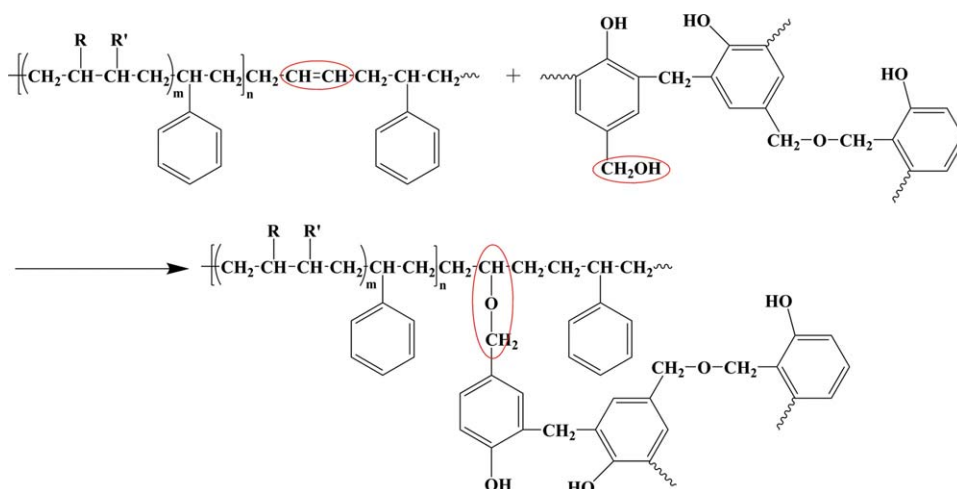
Figure 11. High-resolution O1s XPS spectra: (a) PF, (b) PF/SBR0.5, (c) PF/SBR1.5, (d) PF/SBR2.5, (e) PF/SBR3.0. [Color figure can be viewed in the online issue, which is available at wileyonlinelibrary.com.]

accordance with the analysis of Figure 9(b,c). (2) The relative intensity of peaks on both sides of 1200 cm^{-1} changes. The band 1230 cm^{-1} assigned to C—O—C increases, which may be due to the interaction between —CH$_2$—OH group in PF and C=C bond in SBR. With the increase of temperature, the breakage of C—O—C bond weakens the effect of SBR. (3) The variations in C=C bond at 1640 cm^{-1} and C—O bond of CH$_2$—OH group are small, showing that the possible chemical reaction between SBR and PF is weak. As a result, on the one hand, the association of phenolic hydroxyl groups is broken by rubber macromolecules. On the other hand, a certain chemical interaction may occur between —CH$_2$—OH group in PF and C=C bond in SBR, which promotes the interfacial bonding and the increase of impact strength for phenolic nanocomposites.

Furthermore, to further analyze the formation of C—O—C bond between —CH$_2$—OH group in PF and C=C in SBR, high-

resolution C1s and O1s XPS spectra of PF and PF/SBRX (X = 0.5, 1.5, 2.5, 3.0) are displayed in Figures 10 and 11, respectively. Figure 10 shows that there are two carbon-based functional groups: the peak assigned to C—C in aliphatic and aromatic groups (around 284.8 eV), and the peak attributed to C—O in ether or hydroxy group (around 286.2 eV).[22–24] As the SBR loading increases, the content of C—C bond in phenolic nanocomposites gradually decreases from 84.8 to 62.2% and the content of C—O bond increases from 15.2 to 37.8%, indirectly indicating the C—O—C bond is produced. Figure 11 reveals that there are two oxygen-based functional groups including C—O (ether or hydroxy group, around 532.8 eV),[24] and O—H (hydroxy, around 531.6 eV).[25] With the increase of SBR loading, the content of C—O bond in phenolic nanocomposites gradually increases from 72.9 to 84.7% and the content of O—H bond decreases from 27.1 to 15.3%, showing that the C—O—H bond is converted to C—O—C bond. The analysis of high-

Scheme 1. The interaction between SBR and PF. [Color figure can be viewed in the online issue, which is available at wileyonlinelibrary.com.]

resolution C1s and O1s XPS spectra for PF and PF/SBRX ($X = 0.5, 1.5, 2.5, 3.0$) further confirms the speculation of FTIR spectra that there exists a weak chemical interaction between SBR nanoparticles and the PF matrix, as shown in Scheme 1. Thus, the chemical interaction may be responsible for the compatibility and the transition layer between SBR nanoparticles and the PF matrix, and promotes the formation of good interface. Accordingly, the impact strength of phenolic nanocomposites is significantly improved without sacrificing the flexural performance, and the thermal decomposition temperature of phenolic nanocomposites is not affected significantly.

CONCLUSION

The mechanical and thermal properties of phenolic nanocomposites, and the toughening mechanism were studied in detail. Based on the experimental results, the following conclusions can be drawn:

1. The phenolic nanocomposites modified with SBR nanoparticles possessed good comprehensive mechanical properties. The notched impact strength of phenolic nanocomposites with 2.5 wt % SBR nanoparticles was increased by 52%, compared with pure PF. Meanwhile, the flexural strength was improved and the flexural modulus only declined slightly. Moreover, SBR nanoparticles had little influence on the thermal decomposition temperature of phenolic nanocomposites.
2. The certain compatibility between SBR nanoparticles and the PF matrix, which might be due to the weak chemical interaction between SBR nanoparticles and the PF matrix, played a key role in the enhancement of impact strength for phenolic nanocomposites.
3. Phenolic nanocomposites possessed a two-phase structure with the uniform dispersion of SBR nanoparticles at a nanoscale and there was a critical interparticle distance between PF/SBR2.5 and PF/SBR3.0. Furthermore, there existed a transition layer with a thickness of about 15 nm between

SBR nanoparticles and the PF matrix, which might be responsible for the good interfacial bonding and the great enhancement of the toughness for phenolic nanocomposites.

REFERENCES

1. Choi, M. H.; Byun, H. Y.; Chung, I. J. *Polymer* **2002**, *43*, 4437.
2. Situ, Y.; Hu, J. F.; Huang, H.; Fu, H. Q.; Zeng, H. W.; Chen, H. Q. *Chin. J. Chem. Eng.* **2007**, *15*, 418.
3. Cardona, F.; Kin-Tak, A. L.; Fedrigo, J. *J. Appl. Polym. Sci.* **2012**, *123*, 2131.
4. Goswami, S.; Maji, S. K. *J. Appl. Polym. Sci.* **2012**, *123*, 3007.
5. Kaynak, C.; Cagatay, O. *Polym. Test.* **2006**, *25*, 296.
6. Yang, T. P.; Kwei, T. K.; Pearce, E. M. *J. Appl. Polym. Sci.* **1990**, *41*, 1327.
7. Matsumoto, A.; Hasegawa, K.; Fukuda, A.; Otsuki, K. *J. Appl. Polym. Sci.* **1992**, *44*, 1547.
8. Ma, H. Y.; Wei, G. S.; Liu, Y. Q.; Zhang, X. H.; Gao, J. M.; Huang, F.; Tan, B. H.; Song, Z. H.; Qiao, J. L. *Polymer* **2005**, *46*, 10568.
9. Yu, Z.; Li, J. F.; Yang, L. M.; Yao, Y. L.; Su, Z. Q.; Chen, X. N. *J. Appl. Polym. Sci.* **2012**, *123*, 1079.
10. Qi, G. C.; Zhang, X. H.; Li, B. H.; Song, Z. H.; Qiao, J. L. *Polym. Chem.* **2011**, *2*, 1271.
11. Huang, F.; Liu, Y. Q.; Zhang, X. H.; Gao, J. M.; Song, Z. H.; Tang, B. H.; Wei, G. S.; Qiao, J. L. *Sci. China Ser. B* **2005**, *48*, 148.
12. Derakhshandeh, B.; Shojaei, A.; Faghihi, M. *J. Appl. Polym. Sci.* **2008**, *108*, 3808.
13. Li, D. S.; Xia, H. B.; Peng, J.; Zhai, M. L.; Wei, G. S.; Li, J. Q.; Qiao, J. L. *Radiat. Phys. Chem.* **2007**, *76*, 1732.
14. Zhan, M. S.; Xiao, W.; Li, Z. *J. Aeronautical Mater.* **2003**, *23*, 34.
15. Laura, D. M.; Keskkula, H.; Barlow, J. W.; Paul, D. R. *Polymer* **2003**, *44*, 3347.

16. Liu, X. B.; Lina Bian, L. N.; Gao, Y.; Wang, Z. *Polym. Bull.* **2012**, *69*, 747.

17. Mertz, G.; Hassouna, F.; Leclère, P.; Dahoun, A.; Toniazzo, V.; Ruch, D. *Polym. Degrad. Stab.* **2012**, *97*, 2195.

18. Zhan, M. S.; Wang, Y.; Fang, Y. *China Plast.* **1997**, *11*, 14.

19. Gietl, T. D.; Lengsfeld, H. D.; Altstädt, V. D. *J. Mater Sci.* **2006**, *41*, 8226.

20. Zhang, Y. D.; Lee, S.; Yoonessi, M.; Liang, K. W.; Pittman, C. U. *Polymer* **2006**, *47*, 2984.

21. Carotenuto, G.; Nicolais, L. *J. Appl. Polym. Sci.* **1999**, *74*, 2703.

22. Wang, X.; Hu, Y.; Song, L.; Xing, W. Y.; Lu, H. D.; Lv, P.; Jie, G. X. *Polymer* **2010**, *51*, 2435.

23. Gelius, U.; Heden, P. F.; Hedman, J.; Lindberg, B. J.; Manne, R.; Nordberg, R.; Nordling, C.; Siegbahn, K. *Phys. Scripta.* **1970**, *2*, 70.

24. López, G. P.; Castner, D. G.; Ratner, B. D. *Surf. Interface Anal.* **1991**, *17*, 267.

25. Park, S. J; Jang, Y. S. *J. Colloid Interface Sci.* **2001**, *237*, 91.